Enhanced electrochemical performance of copper vanadate nanorods as an electrode material for pseudocapacitor application

S. EzhilArasi[1] · R. Ranjithkumar[1] · P. Devendran[1] · M. Krishnakumar[1] · A. Arivarasan[1]

Abstract

Copper vanadate nanorods were synthesized by simple chemical route and its electrochemical performances were investigated. X-ray diffraction and Fourier transform infrared spectroscopy analyses showed that the copper vanadate nanorods were composed of nano monoclinic crystalline structure having $Cu_3V_2O_8$ phase with metallic bond vibrations. Observations from scanning electron microscopic and high-resolution transmission electron microscopic studies revealed the rod like morphology of copper vanadate with ∼ 200 nm size. Pseudocapacitive behaviour possessed by pristine $Cu_3V_2O_8$ nanorods was investigated by electrochemical analyses such as cyclic voltammetry, chronopotentiometry and electrochemical impedance spectroscopic techniques using aqueous alkaline electrolyte. Elemental composition with overall atomic distribution was elucidated by energy dispersive spectroscopy combined with elemental mapping. Based on the results, $Cu_3V_2O_8$ nanorods was proved to be a promising electrode material for pseudocapacitors, as it delivered eminent specific capacitances of 430 Fg^{-1} at the current density of 0.4 $mAcm^{-2}$, and 497 Fg^{-1} at the scan rate of 5 mVs^{-1}. It possesses reasonable cycling stability of 94.7% capacitance retention and superior coulombic efficiency after 5000 charge–discharge cycles at 4 Ag^{-1}.

1 Introduction

The ultimate progress in population rate has made energy crisis all around the world which at the same time leads to high energy demand. Now, energy production and storage is major need along with the improvements in technologies [1, 2]. In order to make some energy conversion/storage devices with high power and energy densities, electrochemical devices have been fabricated and made commercial all over the world. But unfortunately few existing conventional energy conversion/storage devices available in market with many drawbacks that surreptitiously affects and pollutes the environment [3]. Electrochemical cells like batteries, supercapacitors and fuel cells serve as an excellent alternative eco-friendly energy sources that paved way for present generation of power production [4, 5]. Among this, supercapacitors are found to have high power density, long life span with cyclic stability, etc. [6–8].

The mechanism of charge storage in supercapacitor is divided into two categories such as non-faradaic process (electrochemical double layer capacitors, EDLCs) and faradaic process (pseudocapacitors, PCs) [9–11]. In non-faradaic process, ions from electrolyte undergoes adsorption/desorption on the carbon material having high surface area for storing charge, whereas in faradaic process the electron from conducting polymers or metal oxides store charge through electron transfer process [12, 13]. However, the combination of carbon materials with conducting polymers and metal oxides can also have good charge storage mechanism and hence named it as hybrid capacitors (HCs) [14, 15].

In recent years, comparing metal sulphides [16], hydroxides [17], in-expensive transition metals oxides are attracting more researchers for their lucrative applications in various fields [18–23]. In connection with this, vanadium compound has its unique physical and chemical properties that makes it essential for diverse applications. Besides various vanadate structures like $BiVO_4$ [24], $Zn_3(VO_4)_2$ [25], the copper vanadate is the fascinating inorganic material and has most notable characteristics such as photocatalysis, electrochemical sensing, water splitting, electrochemical as well as photochemical storage and conversion abilities, etc. [26–31]. Apart from this, it also has some special features viz. ecologically harmless, viable etc. Cao et al. has prepared

✉ A. Arivarasan
arivarasan.nanotech@gmail.com

1 International Research Centre, Department of Physics, Kalasalingam Academy of Research and Education, Krishnankoil, Tamilnadu, India

CuV_2O_6 through sol gel method at different temperatures. They examined its electrochemical property and showed its highest discharge capacity of about 403 mAhg^{-1} [32]. Sun et al. has synthesized 3D flower like $Cu_3V_2O_7(OH)_2 \cdot 2H_2O$ compound via surfactant assisted hydrothermal method. Also, Sun et al. had examined its electrochemical performance in various temperatures and revealed better performances of about 326 mAhg^{-1} at 37 °C [33].

Here, this work explores the electrochemical performance elucidation of prepared copper vanadate as a modified electrode material for efficient PCs. As far as we know, there has been no work reported on $Cu_3V_2O_8$ nanorods (CVNRs) as an electrode material for pseudocapacitors. CVNRs can be synthesized via diverse techniques such as hydrothermal [34], solid state reaction [35], thermal decomposition method [36], laser ablation [37] etc., Among those methods, we have chosen easy, cost-effective chemical route method to prepare CVNRs. At the same time, the structural, morphological and optical studies have also been carried out to prove the material characteristics possessed by the calcined CVNRs.

2 Experimental and characterization techniques

2.1 Materials for the synthesis of copper vanadate nanorods (CVNRs)

Preparation of pristine copper vanadate nanorods (CVNRs) was carried out with 99% pure analytical grade chemicals purchased from Sisco Research Laboratories (SRL) Pvt. Ltd., Mumbai, India. The precursors consists of copper(II) nitrate $Cu(NO_3)_2$, ammonium metavanadate (NH_4VO_3), polyvinylpyrolidine (($C_6H_9NO)_n$), PVP), sodium hydroxide (NaOH) and ethanol. Without any further purifications, deionized (DI) water was employed for whole chemical reaction and used as the solvent for electrolyte preparations. Besides this, for electrochemical analysis, potassium hydroxide (KOH), N-methyl-2-pyrrolidinone (C_5H_9NO, NMP) and polyvinylidene fluoride (($-(C_2H_2F_2)_n-$), PVDF) were purchased from Sigma-Aldrich, Mumbai India.

2.2 Material synthesis and characterization

The method employed to synthesis CVNRs was simple co-precipitation method. The concentration of starting materials taken were 0.05 M $Cu(NO_3)_2$ and NH_4VO_3. The nanorods size, growth and pH of the reaction mixture were controlled by adding trace amount (0.05 g) of PVP and 0.05 M of NaOH, respectively under constant stirring. The pH was set to 7. Inorganic reaction occurred in the reaction mixture was given in Eq. (1).

$$3Cu(NO_3)_2 + 2NH_4VO_3 + 3NaOH$$
$$\rightarrow Cu_3V_2O_8 + 3NaNO_3 + 2NH_4OH \qquad (1)$$
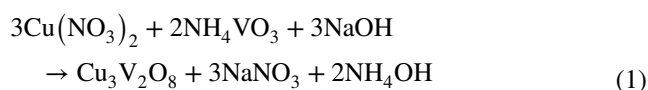
The precipitate acquired after completion of reaction was collected and washed more than five times to remove the un-reactants using DI water and ethanol. Then the dehydration of obtained nanomaterials was done in air oven at 80 °C for 12 h and calcinated at 350 °C for 4 h.

Assisted by Powder X-ray diffraction analysis (PXRD) made of Bruker (D8 advance ECO) which has an X-ray wavelength of 1.5406 Å with monochromatic Cu–K$_\alpha$ radiation, the crystalline structure of synthesized CVNRs were confirmed. The valence and oxidation states of prepared CVNRs were elucidated by X-ray photoelectron spectroscopy (XPS, ULVAC-PHI, Inc; Model: PHI5000 Version Probe III) with the help of Al Kα as the X-ray source. To evaluate the optical properties and functional groups of prepared CVNRs, Shimadzu UV 1800 spectrophotometer and Shimadzu (IR Tracer-100) spectrophotometer combined with KBr pellet system was employed to record UV–Visible (UV–Vis) absorption as well as Fourier transform infrared (FTIR) spectra, respectively. Scanning Electron Microscope (SEM) of ZEISS-EVO 18 Research, Japan and JEOL JEM 2100 h-TEM High-Resolution Transmission Electron Microscope (HR-TEM) was utilized to record the surface and structural morphologies of CVNRs, respectively. The elemental composition with uniform distribution was proved by Energy Dispersive X-ray analysis (EDX) (EDAX-APEX) combined with elemental mapping.

2.2.1 CVNRs modified working electrode construction and electrochemical measurements

Fabrication of CVNRs modified working electrode were carried out by mixing 80% weight percentage of prepared CVNRs and 15% acetylene black and 5% PVDF. Using NMP as a solvent, the mixture was made into a slurry and coated on nickel foil substrate that has an area of about 1 cm^2. The substrate with the slurry was dried overnight in an air oven at a temperature of about 60 °C. In order to analyse the pseudocapacitive nature of prepared electrode, it was examined via electrochemical techniques such as cyclic voltammetry (CV), galvanometric charge–discharge (GCD) and electrochemical impedance spectroscopy (EIS). This was done by an electrochemical workstation (CH Instruments-CHI 6008e, USA) in three electrode system. Fabricated electrode, a platinum (Pt) wire and Ag/AgCl were used as the working electrode, counter electrode, and reference electrode, respectively. 2 M aqueous potassium hydroxide solution was employed as an electrolyte.
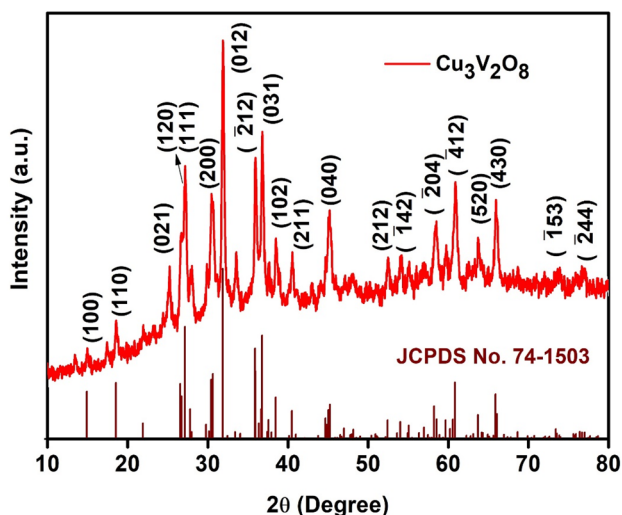
Fig. 1 XRD pattern of CVNRs

Fig. 2 FTIR spectrum of CVNRs

3 Results and discussion

3.1 Material quality analyses of CVNRs

The PXRD pattern of calcinated CVNRs was depicted in the Fig. 1. The 2θ values were fixed between 10° and 80°. Crystal structure examined from PXRD technique was found to be monoclinic structure with $Cu_3V_2O_8$ phase. The space group were observed to be P21/c(14) with cell parameters $a = 6.249$ Å, $b = 7.993$ Å, $c = 6.377$ Å. The peaks show major accordance with bulk copper vanadate (JCPDS File no.#: 74-1503) which was similar to the XRD pattern reported by Arani et al. [38]. The 2θ values that have maximum intense peaks were well aligned to its hkl indices. The formation of minor wider peaks suggests that the prepared CVNRs were in nanometre range. No other supplementary peaks were observed from other phases and it clearly declared that the prepared CVNRs were extremely taintless. Using Scherrer formula given in Eq. (2),

$$D_{hkl} = K\lambda / \beta \cos \theta \tag{2}$$

the grain size of the prepared CVNRs were estimated. D suggest the average crystallite size; Scherrer constant was given as K that has constant value of 0.9, λ implies wavelength of X-ray source, full width at half maximum (FWHM) value of high intensity peaks was mentioned by β and finally θ, the Bragg's diffraction angle. Henceforth, the crystallite size of the prepared CVNRs was aggregated to be ~ 25 nm.

FTIR spectrum recorded in the range between 4000 and 400 cm^{-1} of calcinated CVNRs were shown in Fig. 2. In accordance with the former report, peak at 414.70 cm^{-1} was attributed by stretching vibration of metallic Cu–O bond [38]. The forma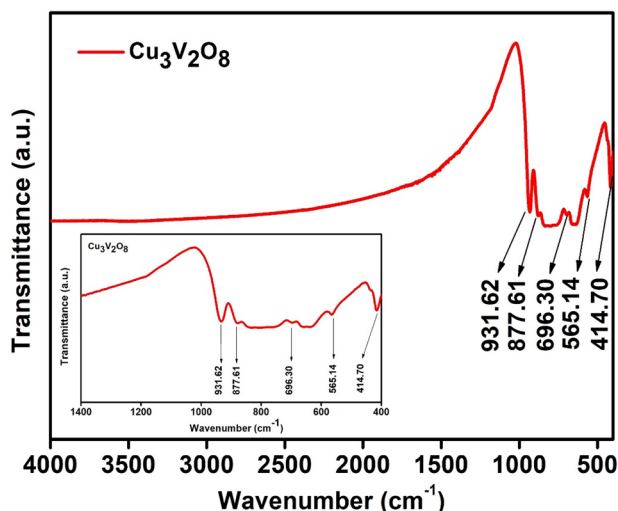tion of bands near 877 cm^{-1}, 696 cm^{-1}, and 565 cm^{-1} were due to the bond vibrations of inorganic V–O–V and VO_4^{3-} interactions. The presence of peaks between 931 and 414 cm^{-1} confirmed the network vibrations of tetrahedral positioned VO_4 and octahedral positioned CuO_6. Appearance of peaks only in finger-print region clearly proved that the prepared CVNRs do not contain any organic and hydroxide materials. This further clarified the purity of the sample and was found to be as same as earlier report [38].

The surface elemental composition and oxidation state binding energies of CVNRs were analysed with XPS spectra depicted in Fig. 3a–e. The full survey spectrum confirmed the presence of Cu2p, V2p, O1s and C1s elemental peaks with their binding energies of 954.7, 934.7, 517 eV, 524.2, 530.1 and 517 eV, respectively, and no impurities could be found on the surface of prepared CVNRs. All high-resolution (HR) spectra were corrected with reference carbon C1s peak at 285 eV and closely fitted with Gaussian fitting. The Cu2p peaks located with their binding energies at 934.7 and 954.7 eV correspond to $Cu2p_{3/2}$ and $Cu2p_{1/2}$ with the splitting energy of 20 eV and in connection two notable shakeups were observed in between 941–943.6 eV, designated that Cu^{2+} was the dominant oxidation state [39, 40]. Moreover, appearances of two minor peaks positioned at 943.6 and 941 eV were attributed to the satellite shakeup of Cu(II) open $3d^9$ shell [41]. Similarly, the HR spectrum of V2p band traced at the binding energies of 517 eV and 524.2 eV due to $V2p_{3/2}$ and $V2p_{1/2}$ states, respectively, with spin orbit coupling values of about 7.2 eV between them. The binding energy of V2p states was ascribed by the elemental interaction of vanadium with oxygen. The peak broadness of $V2p_{3/2}$ clearly indicated the combination of two different V^{4+} and V^{5+} ion oxidation states [42]. Eventually, the deconvoluted O1s (oxygen) profile shown in Fig. 3e had two peaks at

Fig. 3 XPS spectra of CVNRs **a** wide scan spectrum **b** deconvolution of C1s spectrum **c** deconvolution of Cu2p **d** deconvolution of V2p **e** deconvolution of O1s spectrum
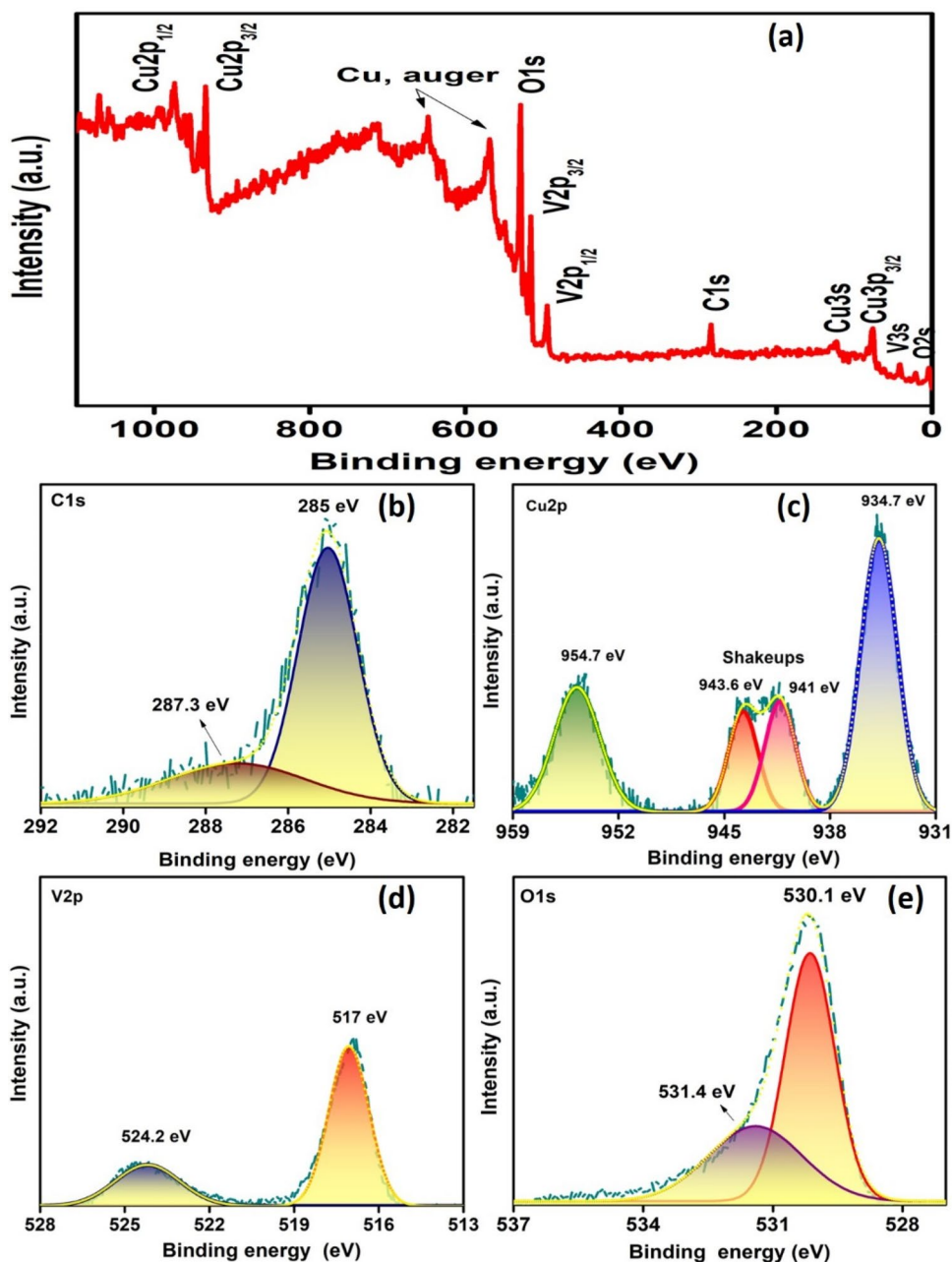
530.1 and 531.4 eV. The appearance of these peaks might be due to the M–O (O^{2-} lattice oxygen) and defects (oxygen defects, chemisorbed oxygen), respectively. This results which was in accordance with EDS result (Fig. 6a) clearly stated the purity of prepared CVNRs.

The UV–Vis absorption spectrum of calcinated CVNRs was delineated in Fig. 4. Presence of binary metals in the prepared CVNRs was confirmed through the appearance of two broad absorption shoulder peaks at 262 and 325 nm. Appearance of absorption peak at 262 nm was attributed by the excitonic absorption of copper-oxygen interaction whereas the absorption maximum at 325 nm was contributed by the presence of vanadium and oxygen interaction.

The wider peak implies that the prepared material size was in nano range. This was in coherence with the XRD (Fig. 1) and SEM (Fig. 5) results. It also proved that the CVNRs has good optical characteristics with a photo response in UV region.

The surface and structural morphologies of the prepared CVNRs were examined using SEM and HR-TEM analyses, respectively. Figure 5a, b illustrates the SEM images and Fig. 5c, d shows the HR-TEM images of prepared CVNRs. Mixture of rod- and sphere like morphologies with sizes varying in diverse nano and micro ranges were observed in SEM analyses and it was further confirmed by HR-TEM images. The observation of sphere like morphology
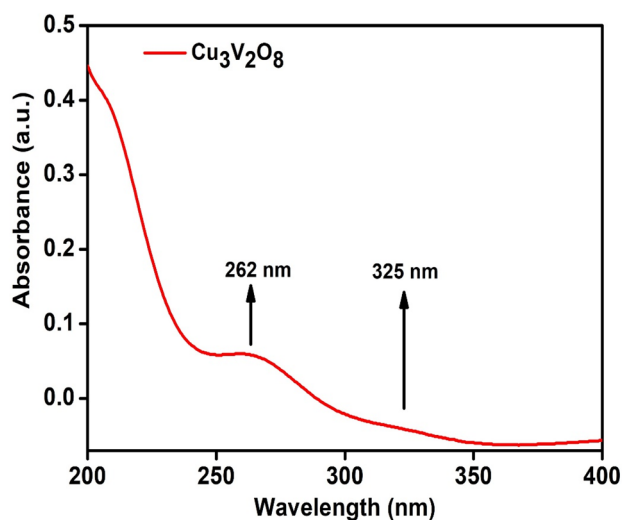
Fig. 4 UV–Vis spectrum of CVNRs

in SEM images may be due to the aerial view of vertical nanorods. Smaller sized particles were combined to form nanorods and it was revealed by HR-TEM analyses. The confirmation of elements in prepared CVNRs was identified by EDS spectrum. The lattice fringes and selective area

electron diffraction (SAED) pattern of prepared CVNRs were depicted in Fig. 5e, f. The single crystalline nature was confirmed from the lattice fringes. The obtained SAED pattern was in good agreement with XRD results and proved the monoclinic structure of crystal.

Figure 6a reveals EDS spectrum of the prepared CVNRs that contains only Cu, V and O elements with weight percentage in accordance with the XRD result (Fig. 1). In addition, the purity of prepared CVNRs was furthermore confirmed through the absence of additional elemental peaks. From the Fig. 6b–e, the distribution of elements was confirmed to be in even through the mapping analysis.

3.2 Pseudocapacitive evaluation

The electrochemical behaviour and supercapacitive nature of prepared CVNRs in aqueous medium were determined by utilizing CV measurements, GCD analysis and EIS technique.

3.2.1 CV

The CV studies had been carried out to estimate the redox property of prepared CVNRs modified electrode. Figure 7a demonstrated the sequential CV curves of modified CVNRs
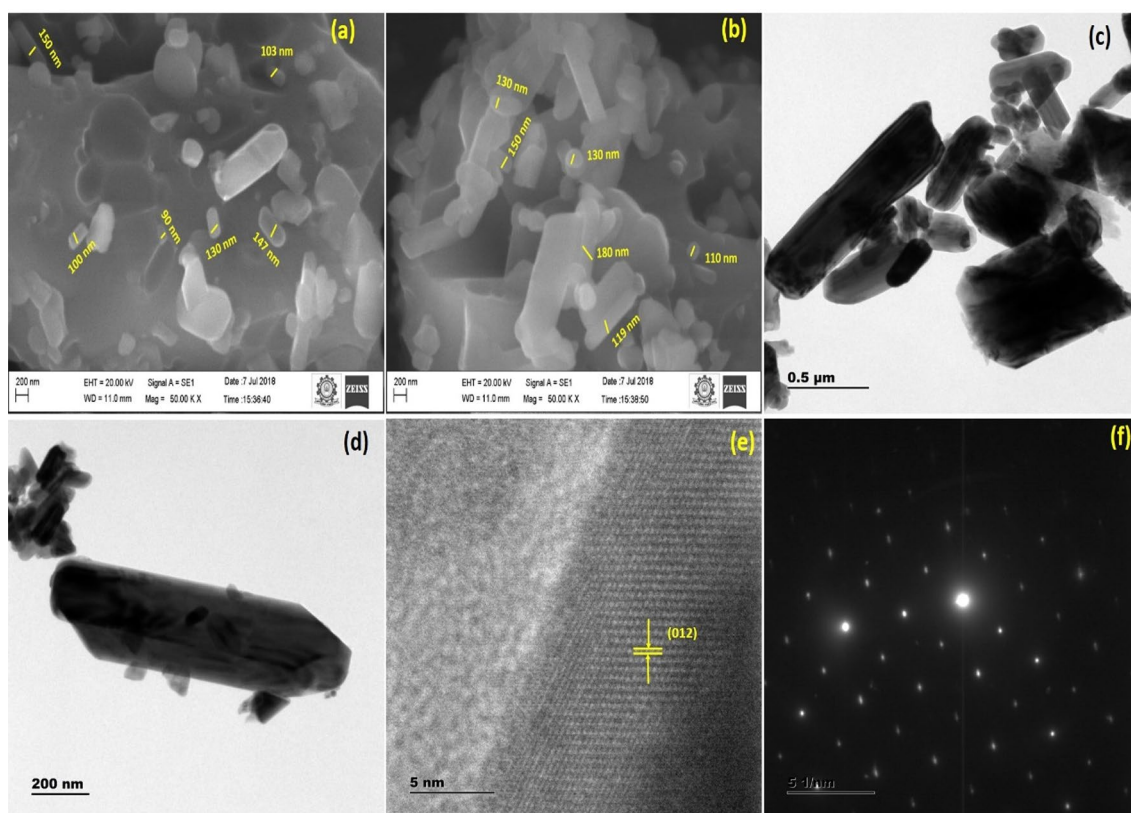

Fig. 5 **a**, **b** SEM images of CVNRs and **c**, **d** HR-TEM images of CVNRs. **e**, **f** Fringes and SAED pattern revealing higher crystallinity
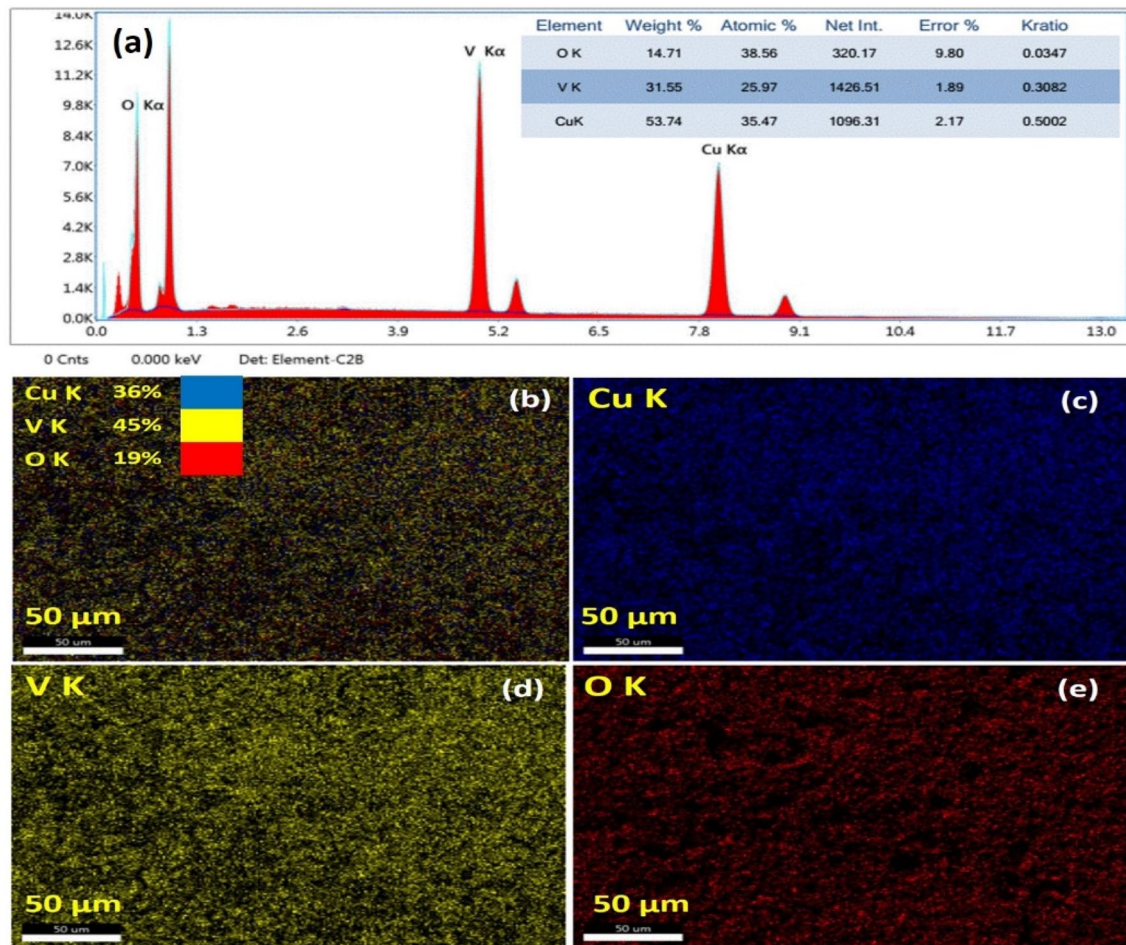
Fig. 6 **a** EDS spectrum, **b–e** Elemental mapping of CVNRs

electrode at diverse sweep rates. The current frame was assigned between $+0.04$ and -0.04 Ag^{-1} with respect to potential window fixed between 0 and 0.6 V. The pair of redox humps at anode, cathode area clearly denoted that the prepared CVNRs modified electrode was electrochemically active and had underwent reversible redox mechanism. By the result of faradaic redox reaction between metal, metal oxides and metal hydroxides, this peak had been emerged [15]. At all sweep rates from 100 to 5 mVs^{-1}, rather than the minor shifts there had been no changes in shape of the CV curve.

The comparison between 1st and 1500th curves of CV cycle was depicted in Fig. 7b. Similar pattern with minor changes were observed. This reconfirmed the prepared modified CVNRs working electrode was electrochemically stable. The minor changes in CV curve were due to the sudden agitation of ions during diffusion process after cycling test. Because of internal resistance, the minor shift had been entertained in both sides of curve. Under slow sweep rate, the specific capacitance value was found to be higher and vice versa which was depicted in the Fig. 7c. The specific

capacitance values were calculated from the Eq. (3) and listed in Table 1. The square roots of scan rate and peak currents were in the linear relationship which was showed as randles plot in Fig. 7d.

$$C_{sp} = \frac{1}{vm(V_a - V_c)} \int_{V_a}^{V_c} I(V)dV \, (Fg^{-1})$$ (3)

where specific capacitance $-C_{sp}$, υ specified the scan rate, m indicated the mass of the active material, I correspond to the current, V denoted the potential window, V_c and V_a were the voltage window of cathodic and anodic region, respectively.

3.2.2 GCD

The GCD curve of prepared CVNRs was shown in Fig. 8a and the specific capacitance differences were given in Fig. 8b. The charge–discharge curves were recorded for different current densities ranging from 0.5 to 4 Ag^{-1} between the potential window 0 and 0.5 V. In general, the linear charge–discharge curves suggest the pseudocapacitive
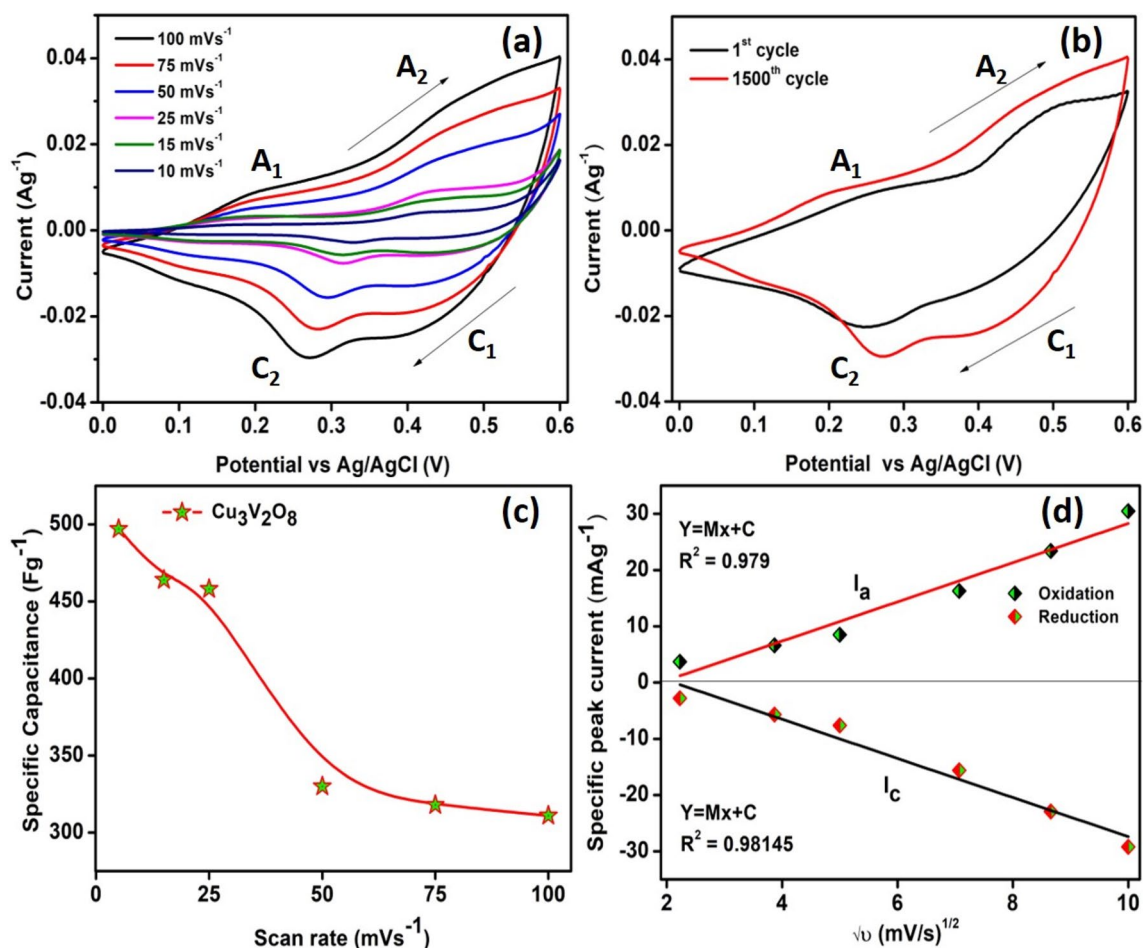
Fig. 7 **a** CV curve of CVNRs modified electrode at various scan rate, **b** CV curves of 1st and 1500th cycle, **c** Relation between specific capacitance and scan rates, **d** Randles plot obtained for the CVNRs modified electrode in 2M KOH

Table 1 Evaluated specific capacitance values for CVNRs using different scan rate from obtained CV curves

S. no	Scan rate (mV s^{-1})	Specific capacitance (Fg^{-1})
1	5	497
2	15	464
3	25	458
4	50	330
5	75	318
6	100	311

behaviour of the material. This particular nature was observed in prepared CVNRs in which the adsorption and desorption process were attributed by the charge storage mechanism of CVNRs. Usually the charge–discharge curves consist of three different parts occurred due to the internal resistance, separation of ions between electrode/electrolyte interface and redox property of the prepared CVNRs. The specific capacitance values were calculated from Eq. (4) and

listed in Table 2. On increasing the current density values, the discharge time decreased simultaneously which was reflected through changes in the specific capacitance values.

$$C_{\mathrm{sp}} = \frac{I\Delta t}{m\Delta V} \left(\mathrm{Fg}^{-1}\right) \tag{4}$$

where I referred the current, Δt indicated the discharge time, m denoted the mass of active material, V specified the potential window or voltage window.

The cyclic stability of the prepared CVNRs were examined by subjecting continuous 5000 charge–discharge cycles at current density of 4 Ag^{-1}. Figure 9 shows the capacitive retention and coulombic efficiency of the prepared CVNRs. A gradual decrease in specific capacitive retention value after 1600th cycle was noted from 100 to 94.7% via the cyclic test which might be due to the minor degradation of the active material. Also, at around 4200th cycle the interaction of ions in active material with electrolyte were actively participated that resulted in higher retention values. The coulombic efficiency of about 99% was achieved at the end of
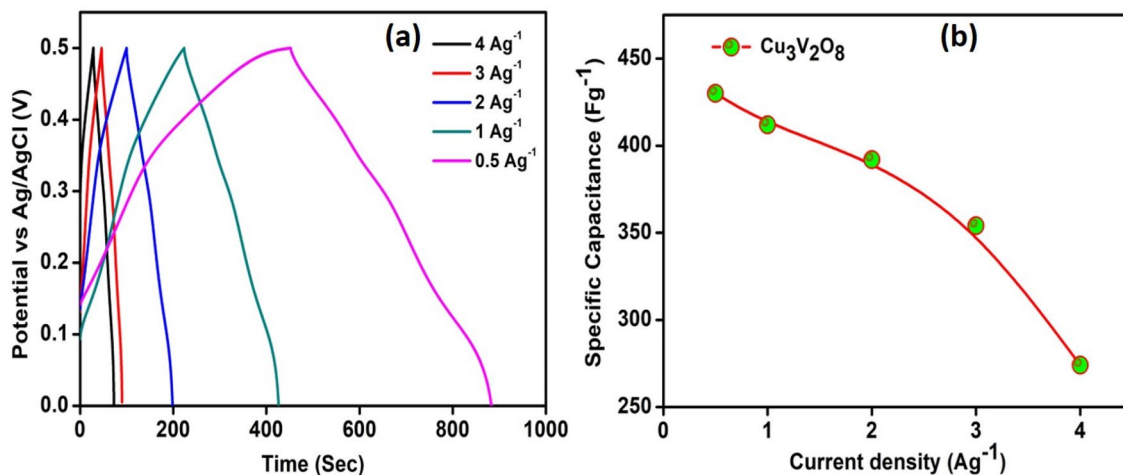
Fig. 8 **a** GCD curve of CVNRs modified electrode with different current densities, **b** variation of current density vs specific capacitance of CVNRs

Table 2 Specific capacitance values of CVNRs modified electrode for various current densities

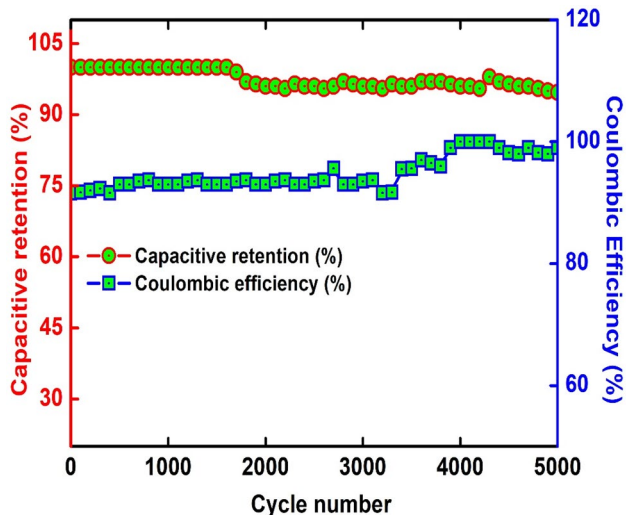| S. no	Current densities (Ag^{-1})	Specific capacitance (Fg^{-1})
1	0.5	430
2	1	412
3	2	392
4	3	354
5	4	274

Fig. 9 Capacitive retention and coulombic efficiency comparison of CVNRs modified electrode
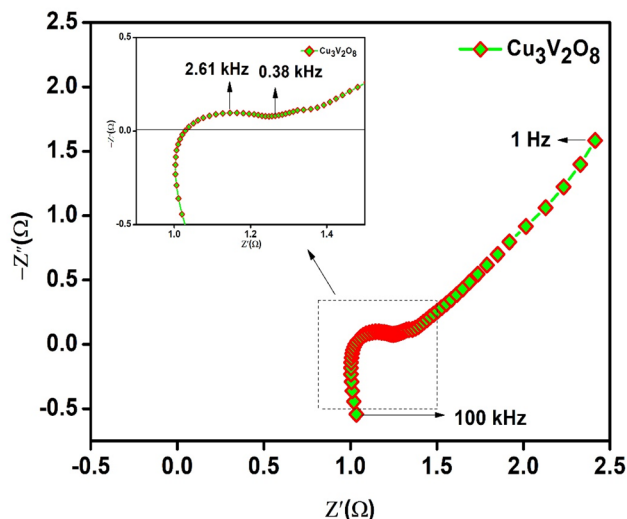

Fig. 10 Electrochemical impedance spectrum (EIS) of CVNRs modified electrode (Nyquist plot)

5000th cycle. It clearly confirmed the stability of prepared electrode material.

3.2.3 EIS

Figure 10 shows the Nyquist plot for CVNRs recorded under open circuit potential. The two major parts in Nyquist plot consist of small semicircle in high frequency region and an inclined slope in low frequency region. At higher frequencies the inductance effects can be noted for semi-conducting electrode materials. Here the appearance of inductance at higher frequency region was due to the high ion conduction in electrolyte with the electrode [43]. Usually the semicircle was attributed by series resistance in interfacial layer and

charge transfer resistance in surface of electrode, while the slope was assigned by the diffusion of ions within the electrodes. The series resistance value was found to be ~ 1.04 Ω whereas the charge transfer resistance was observed at ~ 1.3 Ω. The smaller diameter range of semicircle indicates lower resistance of the CVNRs electrode which was indicated in inset of Fig. 10. Also, the straight inclined slope clearly specified the lower diffusion resistance along with improved capacitive nature of the prepared CVNRs modified electrode.

4 Conclusion

In conclusion, simple chemical route technique had been employed for synthesizing the CVNRs. The calcined CVNRs possessed monoclinic structure with the crystallite sizes of ~ 25 nm. The atomic bond interactions and vibrations between Cu, V and O elements were confirmed through FTIR analysis. Absence of additional organic, inorganic compounds was proved from the FTIR spectrum which was also in correspondence with the EDS spectrum. XPS analysis confirmed the formation of CVNRs with its oxidation states. The particles uniformity, purity and distribution of elements were noticed from EDS and mapping analysis. The nanorod morphology was observed through SEM and HR-TEM images. The absorption maximum observed at 262 nm and 325 nm confirmed optical behaviour of prepared CVNRs. Fast faradaic redox nature and charge–discharge mechanism of prepared CVNRs were investigated along with the cyclic stability test. EIS analysis confirmed the better electrical conductivity and quick charge transfer mechanism. The enhanced electrochemical behaviour suggests that the prepared CVNRs have great potential as a modified electrode material for supercapacitors and energy storage devices.

Compliance with ethical standards

Conflicts of interest The authors declare that they have no conflicts of interest.

References

1. S. Chu, A. Majumdar, Nature **488**, 294 (2012)
2. S. Shafiee, E. Topal, Energy Policy **37**, 181 (2009)
3. H. Ibrahim, A. Ilinca, J. Perron, Renew. Sustain. Energy Rev. **12**, 1221 (2008)
4. M. Winter, R.J. Brodd, Chem. Rev. **104**, 4245 (2004)
5. Y. Wang, Z. Chang, M. Qian, T. Lin, F. Huang, Chem. Eng. J. **375**, 122054 (2019)
6. A. González, E. Goikolea, J.A. Barrena, R. Mysyk, Renew. Sustain. Energy Rev. **58**, 1189 (2016)
7. W.K. Chee, H.N. Lim, Z. Zainal, I. Harrison, N.M. Huang, Y. Andou, K.F. Chong, A. Pandikumar, RSC Adv. **7**, 12033 (2017)
8. S.L. Chiam, H.N. Lim, C.Y. Foo, A. Pandikumar, N.M. Huang, Electrochim. Acta **246**, 1141 (2017)
9. Y. Wang, Y. Song, Y. Xia, Chem. Soc. Rev. **45**, 5925 (2016)
10. B.E. Conway, W.G. Pell, J. Solid State Electrochem. **7**, 637 (2003)
11. J.R. Miller, P. Simon, Electrochem. Soc. Interface **17**, 31 (2008)
12. S.L. Chiam, H.N. Lim, S.M. Hafiz, A. Pandikumar, N.M. Huang, Sci. Rep. **8**, 3093 (2018)
13. F.Y. Ban, S. Jayabal, A. Pandikumar, H.N. Lim, N.M. Huang, Electrocatalysis **6**, 373 (2015)
14. H.A. Abdul Bashid, H.N. Lim, S. Kamaruzaman, S. Abdul Rashid, R. Yunus, N.M. Huang, C.Y. Yin, M.M. Rahman, M. Altarawneh, Z.T. Jiang, P. Alagarsamy, Nanoscale Res. Lett. **12**, 246 (2017)
15. Y. Li, R.B. Kaner, M. Zhu, H. Wang, B. Dunn, Q. Zhang, J. Sun, M.F. El-Kady, Y. Shao, Chem. Rev. **118**, 9233 (2018)
16. K. Jeyabanu, P. Devendran, A. Manikandan, R. Packiaraj, K. Ramesh, N. Nallamuthu, Phys. B Condens. Matter **573**, 92 (2019)
17. P. Vinothbabu, P. Elumalai, J. Solid State Electrochem. **19**, 813 (2015)
18. M. Thiruppathi, M. Vahini, P. Devendran, M. Arunpandian, K. Selvakumar, C. Ramalingan, M. Swaminathan, E.R. Nagarajan, J. Nanosci. Nanotechnol. **19**, 7026 (2019)
19. H. Geng, Q. Zhou, J. Zheng, H. Gu, RSC Adv. **4**, 6430 (2014)
20. P. Chaudhari, S. Mishra, J. Mater. Sci. Mater. Electron. **29**, 117 (2018)
21. Y. Zhang, L. Li, H. Su, W. Huang, X. Dong, J. Mater. Chem. A **3**, 43 (2015)
22. S. Dang, Z. Wang, W. Jia, Y. Cao, J. Zhang, Mater. Res. Bull. **116**, 117 (2019)
23. S. Pilban Jahromi, A. Pandikumar, B.T. Goh, Y.S. Lim, W.J. Basirun, H.N. Lim, N.M. Huang, RSC Adv. **5**, 14010 (2015)
24. R. Packiaraj, P. Devendran, S. Asath Bahadur, N. Nallamuthu, J. Mater. Sci. Mater. Electron. **29**, 13265 (2018)
25. S. Ezhil Arasi, P. Devendran, R. Ranjithkumar, S. Arunpandiyan, A. Arivarasan, Mater. Sci. Semicond. Process. **106**, 104785 (2020)
26. T. Hillel, Y. Ein-eli, J. Power Sources **229**, 112 (2013)
27. L. Zhou, Q. Yan, J. Yu, R.J.R. Jones, N. Becerra-Stasiewicz, S.K. Suram, A. Shinde, D. Guevarra, J.B. Neaton, K.A. Persson, J.M. Gregoire, Phys. Chem. Chem. Phys. **18**, 9349 (2016)
28. W. Guo, W.D. Chemelewski, O. Mabayoje, P. Xiao, Y. Zhang, C.B. Mullins, J. Phys. Chem. C **119**, 27220 (2015)
29. J. Ma, S. Ni, J. Zhang, X. Yang, L. Zhang, Phys. Chem. Chem. Phys. **17**, 21442 (2015)
30. M. Woo Kim, B. Joshi, H. Yoon, T.Y. Ohm, K. Kim, S.S. Al-Deyab, S.S. Yoon, J. Alloys Compd. **708**, 444 (2017)
31. T. Kawada, T. Tajiri, H. Yamashita, M. Machida, Catal Sci. Technol. **4**, 780 (2014)
32. J. Qi Cao, X. You Wang, A. Tang, X. Wang, Y. Wang, W. Wu, J. Alloys Compd. **479**, 875 (2009)
33. X. Sun, J. Wang, Y. Xing, Y. Zhao, X. Liu, B. Liu, S. Hou, CrystEngComm **13**, 367 (2011)
34. S. Zhang, S. Peng, R. Hu, S. Ramakrishna, RSC Adv. **5**, 20692 (2015)
35. L.A. Ponomarenko, A.N. Vasil'ev, E.V. Antipov, Y.A. Velikodny, Phys. B Condens. Matter **284–288**, 1459 (2000)
36. V. Sivakumar, R. Suresh, K. Giribabu, R. Manigandan, S. Munusamy, S. Praveen Kumar, S. Muthamizh, V. Narayanan, J. Mater. Sci. Mater. Electron. **25**, 1485 (2014)

37. Y. Liang, P. Liu, H.B. Li, G.W. Yang, CrystEngComm **14**, 3291 (2012)
38. M. Ghiyasiyan-Arani, M. Masjedi-Arani, M. Salavati-Niasari, J. Mater. Sci. Mater. Electron. **27**, 4871 (2016)
39. J. Ghijsen, L.H. Tjeng, J. van Elp, H. Eskes, J. Westerink, G.A. Sawatzky, M.T. Czyzyk, Phys. Rev. B **38**, 11322 (1988)
40. M.C. Biesinger, L.W.M. Lau, A.R. Gerson, R.S.C. Smart, Appl. Surf. Sci. **257**, 887 (2010)
41. M. Kim, B. Joshi, H. Yoon, T.Y. Ohm, K. Kim, S.S. Al-Deyab, S.S. Yoon, J. Alloys Compd. **708**, 444 (2017)
42. N. Van Hoa, T.T.H. Quyen, N.H. Nghia, N. Van Hieu, J.J. Shim, J. Alloys Compd. **702**, 693 (2017)
43. M. Gresil, V. Giurgiutiu, P. S. Building, 1825 (2014).